Solvophobic and Steric Effects of Side Groups on Polymer Folding: Molecular Modeling Studies of Amine-Functionalized *m*-Poly(phenyleneethynylene) Foldamers in Aqueous Solution

Bamidele Adisa and David A. Bruce*

Department of Chemical and Biomolecular Engineering, Clemson University, Clemson, South Carolina 29634-0909

Received: July 1, 2005; In Final Form: August 23, 2005

The folding behavior of five different amine-functionalized *m*-poly(phenyleneethynylene) (*m*-PPE) oligomers containing 24 phenyl rings (12 residues, where a residue includes 2 phenyl rings) in water was examined by using a combination of molecular dynamics (MD) and replica exchange molecular dynamics (REMD) simulation techniques. The REMD method employed the highly parallelized GROMACS MD software and a modified OPLS-AA force field to simulate 44 replicas of each solvated system in parallel, with temperatures ranging from 300 to 577 K. Our results showed that the REMD method was more effective in predicting the helical conformation of the *m*-PPE in water, from an extended structure, than canonical MD methods in the same simulation time. Furthermore, we observed from canonical MD simulations of the explicitly solvated helical *m*-PPEs at 300 K that the radius of gyration, average helix inner diameter, and average helix pitch of the helical structure all pass through a minima when the side group is R = OC_2H_5 as R is changed from R = H through OC_4H_9.

Introduction

A variety of organic polymers, including proteins, are known to fold into conformations, such as helices and sheets, which exhibit long-range order.[1,2] The formation of a given conformation is usually governed by the system temperature as well as the presence of various inter- and intramolecular interactions, such as electrostatic interactions, hydrogen bonding, and van der Waals (hydrophobic and hydrophilic) interactions.[3] Despite recent advances in experimental techniques, a thorough understanding of the mechanism and dynamics of polymer folding and secondary structure formation still remains an elusive goal for researchers.[4−9] An understanding of these folding phenomena could lead to significant advances in the areas of heterogeneous catalysis, drug delivery, and chemical sensing. It could also provide insight into ailments such as Alzheimer's and Prion diseases (e.g., Creutzfeldt−Jakob disease), which are known to be caused by the misfolding of proteins.[4,10−13]

To provide a better understanding of the intrasolute and solute−solvent interactions of organic polymers, a number of researchers have performed experimental studies on a unique class of nonbiological polymers, *m*-poly(phenyleneethynylene)s or *m*-PPEs (example shown in Figure 1), with varying functional groups, in a variety of solvents.[2,14−23] Specifically, Moore and others[2,14−17] observed that ester-functionalized *m*-PPEs experienced a solvent-driven transition from a random conformation to a helical conformation when the solvent was changed from chloroform to acetonitrile. Similarly, Tew and others[18−20] investigated the conformational changes of amphiphilic *m*-PPEs in solution. They reported that these polymers exhibited different conformational changes depending on the presence or absence of an alkoxy side group when the solvent was changed from DMSO to 90% H_2O/DMSO.[19] In addition, Tan et al.[21] showed via spectroscopic measurements that sulfite functionalized *m*-PPE oligomers (*m*-PPE-SO_3), which are conjugated polyelectrolytes, adopt a helical conformation in water and a random-coil conformation in methanol.

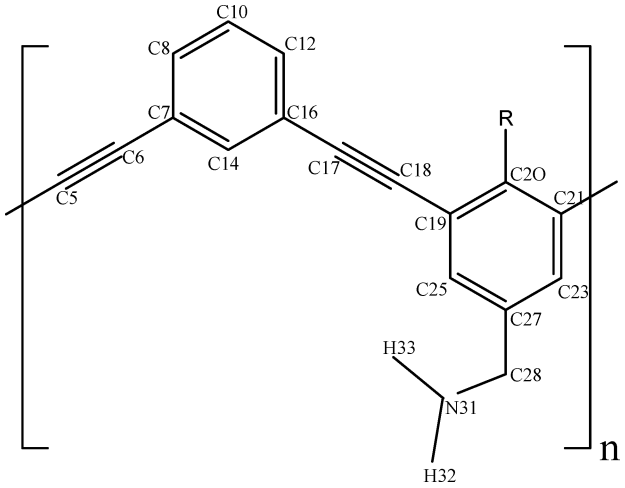

Figure 1. Monomeric unit of the *m*-PPE oligomer. C5 is connected to C21 of the previous unit, while C21 is connected to C5 of the next unit. R = H, $O(CH_2)_xCH_3$, where x = 0 to 3.

Experimental and computational studies[24−27] have also been performed on ortho-linked PPEs (*o*-PPEs). Though the results of these studies suggest that the ortho-linked polymers can also adopt helical conformations in solvents of appropriate polarity, there is a reduction in the free energy of folding brought about by increased steric interactions and the ring strain experienced by these systems upon folding into helical structures. While the aforesaid experimental studies showed that *m*-PPEs adopt a helix conformation in solvents of appropriate polarity, a detailed atomistic investigation of the various interactions that cause these polymer systems to adopt specific conformations was not

* Address correspondence to this author. E-mail: dbruce@clemson.edu. Phone: 864-656-5425. Fax: 864-656-0784.

10.1021/jp053607g CCC: $30.25
Published on Web 10/04/2005

done. Ordinarily, it is difficult to investigate the significance of each of these interactions via experiments, therefore, the need for atomic-level computational studies of these folding phenomena.

Monte Carlo (MC) and molecular dynamics (MD) techniques have become powerful tools for investigating and obtaining relevant atomic-level information about complex chemical systems. Though MC methods have been successfully used to sample the configurational space for protein and polymer systems, this text describes the use of MD and REMD techniques for modeling these systems. MD methods involve numerically solving Newton's equations of motion for a system of atoms that are interacting via a potential that is described by a force field equation.[28,29]

One major problem with traditional MD techniques in investigating the configurational space of a system is that at lower temperatures, the system tends to get trapped in one of the many local minimum energy states; thus, a poor sampling of configurational space is achieved. Several attempts have been made to improve the conformational sampling of complex systems.[30−39,41,42] For example, MD techniques employing simulated annealing[36−38] methodologies have been used to model molecular systems that would otherwise become trapped in configurations unlike that of the global energy minimum. However, the rapid cooling experienced with this approach often traps the system in unrepresentative high-energy conformations. Another more successful approach is the replica exchange molecular dynamics (REMD) technique.[39] In this method, copies (replicas) of the system are simulated independently and simultaneously at different temperatures, and at regular intervals, exchange of configuration between thermally adjacent replicas is attempted. Acceptance of an exchange is based on the Metropolis criterion.[40] This exchange enables a replica to escape local energy minima by exchanging configuration with a higher temperature replica. This method has recently been used to study the folding behavior of biomolecules, including proteins.[39,41,42]

Despite the possible limitations of traditional MD methods described above, a limited number of canonical MD simulation studies have provided key insights into the behavior of *m*-PPE oligomers with varying functional groups in aqueous solvents.[2,43−46] All of these studies showed that appropriately functionalized *m*-PPEs readily adopt a helix conformation in water. In a previous study,[46] we presented results of conventional MD simulations of extended, coiled, and helical *m*-PPE oligomers having alkoxy and amine side groups in water. Though these results showed that the helix structure is the preferred conformation, 5 ns of canonical MD simulation at 300 K of the extended oligomer was not sufficiently long to allow for complete folding of the *m*-PPE into a helix conformation because it quickly became trapped in a local minimum energy conformation.

In an effort to overcome phase sampling problems, we initiated efforts to use a highly parallelized replica exchange molecular dynamics technique to study the aqueous folding behavior of *m*-PPEs, similar to those examined in our previous study, using the GROMACS (version 3.1.4) MD simulation engine[47−49] and a modified version of the OPLS-AA force field.[50−53] We used solvated systems of three different *m*-PPEs, which varied only in the nature of the side group, R (see Figure 1, R = H, OCH_3, and OC_4H_9). A total of 44 replicas of each solvated system were simulated in parallel with temperatures ranging from 300 to 577 K. In addition, canonical MD simulations of these systems were performed at 300 K for comparison with the lowest temperature replicas of the REMD simulations. To our knowledge, this is the first explicit atom, replica exchange MD simulations of amine-functionalized *m*-PPEs in water. Further, we show that the REMD method predicts the helix conformation from an extended structure much more efficiently than conventional MD methods.

The effects of the size of the side group, R, on the conformations adopted by the *m*-PPEs were also investigated in this study. This work complements the experimental studies by Arnt and Tew,[19] which showed that amine-functionalized *m*-PPEs with R = H adopted helical conformations in aqueous solution, whereas *m*-PPEs having long alkoxy substituents (R = $OC_{12}H_{25}$ or greater) were more likely to take on nonhelical conformations. Our study goes a step further by relating the size of the R side group to the dimensions and stacking behavior of the resulting helical conformer. To determine the steric effects associated with R side group size, we performed canonical MD simulations on water-solvated systems of the helical *m*-PPEs, with the R varying from H to an alkoxy group 4 carbon atoms long. Our results show that side group hydrophobicity and size play a significant role in determining the dimensions and structure of the resulting *m*-PPE helix.

Methodology

The replica exchange molecular dynamics (REMD) method was implemented by using the approach proposed by Sugita and Okamoto.[39] The system for REMD consists of N independent replicas of the original system, in a canonical ensemble, run in parallel at N different temperatures. An REMD simulation is then realized by performing the following two steps:

(i) Each replica i ($i = 1, 2, ..., N$) is simulated simultaneously and independently at a fixed temperature T_n ($n = 1, 2, ..., N$) for a certain number of MD steps.

(ii) A pair of thermally adjacent replicas is exchanged based on an acceptance probability. The acceptance probability is given by the Metropolis criterion:[40]

$$w_{ij} = \begin{cases} 1 & \text{for } \Delta \le 0 \\ \exp(-\Delta) & \text{for } \Delta > 0 \end{cases} \tag{1}$$

where $\Delta \equiv (\beta_i - \beta_j)(E_j - E_i)$, i and j represent two adjacent replicas, w_{ij} is the acceptance probability for exchange between replicas i and j, $\beta = (k_B T)^{-1}$, k_B is the Boltzmann constant, and E is the system potential energy. Exchange was attempted only between thermally adjacent replicas because the acceptance probability for exchange decreases exponentially with the difference between the two β values.[39] After each exchange, the velocities of all atoms in each replica pair are rescaled uniformly by the square root of the ratio of the two temperatures to ensure that the average kinetic energy is at the appropriate value for the respective replicas, where the magnitude of the system kinetic energy results from the system temperature, T :[39]

$$\langle E_k(p) \rangle_T = \frac{3}{2} N k_B T \tag{2}$$

The result of this exchange is that low-temperature replicas can overcome high energy barriers in the system by exchanging with a replica modeled at a higher temperature.

For the REMD simulations, three different 12-mer (a total of 24 phenyl rings) *m*-PPE oligomers in the extended conformation were investigated in this study, namely LhC0 (R = H), LhC1 (R = OCH_3), and LhC4 (R = OC_4H_9). These structures were generated with Materials Studio 2.1.[54] Each oligomer system was solvated[55] in a rectangular periodic box of SPC[56]

water molecules to a density of 1 kg·L^{-1}, where the distance between the oligomer and the edge of the box was at least 1.5 nm. The solvated systems were first energy-minimized with a steepest descents method, and then further minimized with the L-BFGS method of Nocedal[57] to remove any close contacts between the oligomer and the surrounding water molecules. The resulting energy-minimized systems were the starting configurations for all simulations.

The system potential energy was calculated with the GROMACS version 3.1.4[47−49] implementation of the OPLS-AA force field[50−53] with atom types and partial atomic charges initially assigned, using the default OPLS-AA parameter set. Some charges were later modified to provide closer agreement with those obtained from quantum mechanical (QM) energy minimized structures. The QM minimization was performed with Jaguar 4.0 software,[58] run on an SGI Onyx2 InfiniteReality2 Dual Rack, and employed density functional theory (DFT), using the hybrid B3LYP[59,60] density functional and the 6-31G**[61] split valence basis set. Partial atomic charges were obtained by fitting the electrostatic potential (ESP) to each atom center and constraining it to replicate the molecular dipole. Additionally, a low-energy rotation barrier was added between neighboring phenyl rings so as to more accurately describe the molecular behavior that has been observed experimentally.[62] In all replica exchange and canonical MD simulations, the leapfrog algorithm[63,64] was used to integrate Newton's equations of motion every 2 fs of simulation time.

Periodic boundary conditions were applied and neighbor list generation was performed after every 5 steps. Both Lennard-Jones (LJ) and Coulombic calculations employed a twin-range[48] cutoff method. A cutoff radius of 0.9 nm was used for short-range forces, which were calculated every simulation step, and a cutoff radius of 1.4 nm was employed for long-range forces, which were calculated during neighbor list generation. In each simulation, temperature was controlled by using the Berendsen coupling method,[65] with a coupling constant of 0.1 ps. The *m*-PPE oligomer and water were independently coupled to the heat bath. Initial velocities were randomly assigned from a Maxwell distribution at the selected simulation temperature. The LINCS algorithm[66] was used to constrain all bonds in nonwater molecules, while the SETTLE algorithm[67] was used to constrain all water bond lengths and angles to their equilibrium values.

The replica exchange MD simulations were implemented by using 44 replicas, distributed over 44 processors, with each replica assigned to one processor. The replicas were run at the following temperatures (in Kelvin): 300, 304, 308, 312, 316, 320, 324, 328, 332, 337, 342, 347, 352, 357, 362, 367, 372, 377, 383, 389, 395, 401, 407, 413, 419, 426, 433, 440, 447, 454, 461, 469, 477, 485, 493, 501, 510, 519, 528, 537, 547, 557, 567, and 577. The simulation temperatures of the replicas were selected such that the acceptance ratios between adjacent replicas were approximately between 10% and 30%. Exchanges were attempted every 100 MD steps (0.2-ps interval) and atomic trajectories were stored before each exchange for further analyses.

Constant temperature MD simulations were also performed at 300 K for five different *m*-PPE oligomers, LhC0 (R = H), LhC1 (R = OCH_3), LhC2 (R = OC_2H_5), LhC3 (R = OC_3H_7), and LhC4 (R = OC_4H_9), in the extended conformation. Further, the effect of hydrophobicity and size of the R side group on the helical structures was investigated by performing canonical MD simulations at 300 K of solvated systems of the helical *m*-PPEs (HhC0, HhC1, HhC2, HhC3, and HhC4). All REMD and canonical MD simulations were stopped after 2 and 5 ns, respectively. Representative schematics of the conformations of the extended and helical *m*-PPE oligomers before energy minimization are shown in Figure 2.

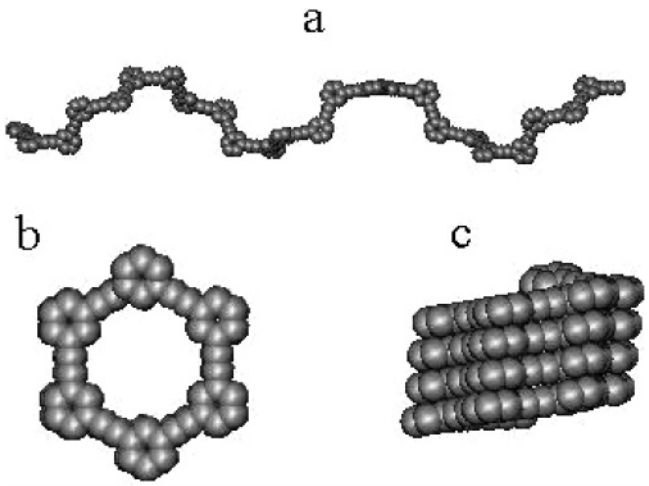

Figure 2. Representative picture of the extended *m*-PPE oligomer before energy minimization (a). Top (b) and side (c) views of the helical *m*-PPE oligomer before energy minimization. Only the oligomer backbones are shown for clarity.

Results and Discussion

The temperature values used in the REMD simulation were chosen to provide reasonable values of the acceptance probability for replica exchange. This was done by performing short trial runs of REMD to determine which temperature intervals would ensure adequate overlap of energies between replicas and consequently enable efficient exchange between replicas. In discussing the REMD results, we will focus attention on one temperature, 300 K, for which we have results from canonical MD simulations available for comparison. We compare the results of replicas of LhC0, LhC1, and LhC4, which finished at 300 K, to the results from canonical MD simulations at 300 K.

The time series for temperature exchange is shown in Figure 3 for the replicas of LhC0, LhC1, and LhC4 that finished at 300 K at the end of the REMD simulations. We observe a random walk in temperature space as these replicas exchange configurations with neighboring replicas. We see that LhC0 (replica 28), which started at 447 K, ended up at 300 K at the end of the simulation. Similarly, LhC1 (replica 28), which started at 447 K, ended up at 300 K, while LhC4 (replica 41), which started at 557 K, ended at 300 K. The temperature profiles show that these replicas move to lower temperatures as they become more compact helical structures and consequently lower energy structures.

Figure 4 shows the oligomer potential energy as a function of simulation time for the REMD and MD simulations. We observe that for the three extended oligomers, steady-state values for the potential energy are attained after about 300 ps for the canonical MD simulations, while for the REMD we observe random walks in the energy profiles that correspond to the temperature profiles for LhC0, LhC1, and LhC4. We can also see that the oligomer structures from REMD simulations finish at lower energies than those from canonical MD simulations and attain energies closer to those of the helix.

This is also seen in Table 1, where the potential energies for LhC0, LhC1, and LhC4 from the REMD simulations are lower than those from the canonical MD simulations. This means that the REMD method enables the *m*-PPE oligomers to overcome

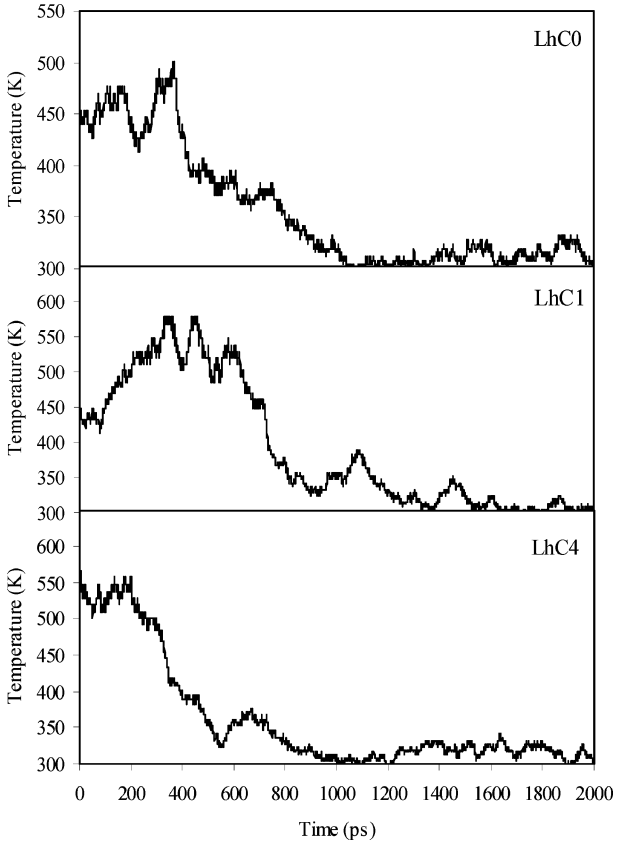

Figure 3. Time series of the temperature exchange from REMD for replicas that finished at 300 K for (a) LhC0, (b) LhC1, and (c) LhC4.

large energy barriers and attain lower energy conformations than the canonical MD method over the same length of simulation time. Furthermore, the low variability of the potential energy for the helix throughout the MD trajectory shows that it did not change considerably from its initial energy-minimized structure, further indicating that it represents the minimum energy conformation for the *m*-PPE oligomer in aqueous solution.[46]

Snapshots of LhC0, LhC1, and LhC4 during the course of the REMD simulations are shown in Figure 5. We see that as the simulations progress, the extended structures are moving toward helical conformations. In particular, LhC4 forms a compact helical structure, in which the hydrophobic alkoxy groups are contained within the core of the structure, and the hydrophilic amine groups are located on the periphery of the structure after approximately 550 ps. Following this initial change in conformation, the oligomer continues to become more organized, which causes a reduction in potential energy, while it slowly becomes the lowest energy replica (i.e., lowest temperature replica), which is modeled at 300 K. This gradual reduction in energy indicates that the oligomer is reducing unfavorable interactions between the alkoxy side chains and water, while maximizing the favorable interactions between the primary amine groups and water. Similarly, we observe a gradual reduction in the potential energies of the LhC0 and LhC1 structures as they first become compact structures and then later transition toward more helical structures. After 2 ns of trajectory, we observe that these structures have formed three complete loops of the helix, suggesting that slightly longer simulations would have enabled the polymers to form complete, well-ordered helical structures.

Figure 6 shows the final structures of LhC0, LhC1, and LhC4 from the canonical MD simulations of the extended oligomers.

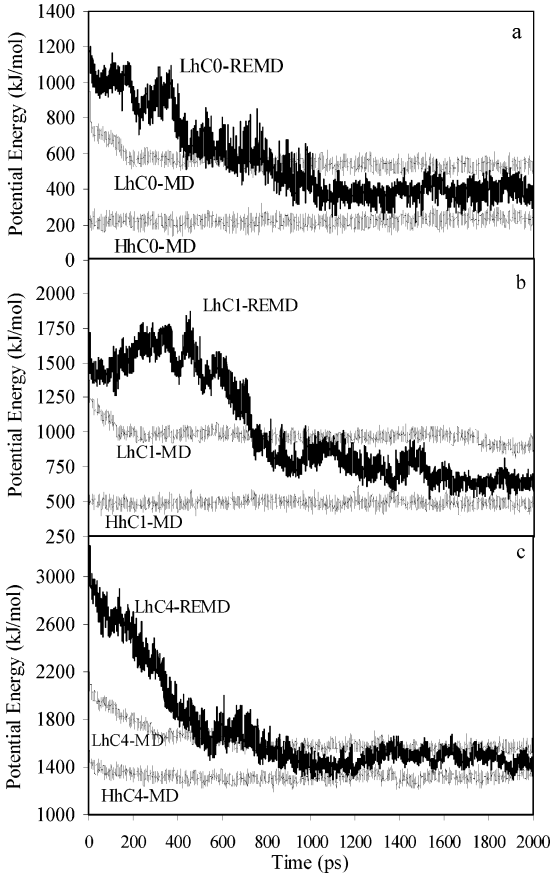

Figure 4. Time series of the potential energy from REMD and MD for (a) extended (LhC0) and helical (HhC0) oligomers with R = H, (b) extended (LhC1) and helical (HhC1) oligomers with R = OCH_4, and (c) extended (LhC4) and helical (HhC4) oligomers with R = OC_4H_9. Only the first 2 ns of MD trajectory is shown.

TABLE 1: Potential Energy from REMD and MD for (a) Extended (LhC0) and Helical (HhC0) Oligomers with R = H, (b) Extended (LhC1) and Helical (HhC1) Oligomers with R = OCH_4, and (c) Extended (LhC4) and Helical (HhC4) Oligomers with R = OC_4H_9, Averaged over the Last 10 ps of Trajectory

	potential energy (kJ/mol)	
structure	REMD[a]	MD[b]
LhC0	359 ± 54	418 ± 32
HhC0		201 ± 32
LhC1	576 ± 31	779 ± 42
HhC1		466 ± 38
LhC4	1376 ± 56	1540 ± 45
HhC4		1339 ± 46

[a] Values after 2 ns of simulation time. [b] Values after 5 ns of simulation time.

We see that random coiled structures are formed after 5 ns of trajectory. Though these structures have fewer unfavorable interactions between the hydrophobic group and water than the extended conformations, they have not fully adopted the optimum helical conformation, indicating that these structures have been trapped in local energy minima. Indeed, we have shown in a previous study[46] that for canonical MD simulations, the initial structure of the extended oligomer affects the final conformation of the oligomer. This effect of initial structure is negligible in the REMD simulations because the exchange between high-temperature and low-temperature replicas enables structures to overcome energy barriers in the system, and therefore, avoid being trapped in local minimum energy states.

The time series for the radius of gyration, R_g, is shown for

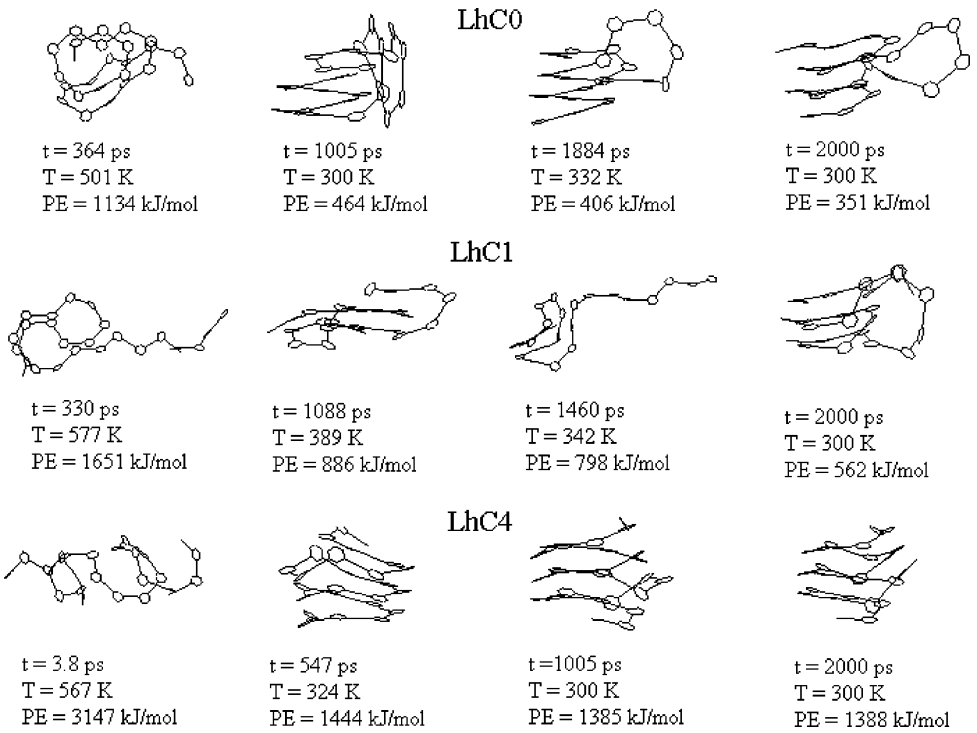

Figure 5. Snapshots of LhC0, LhC1, and LhC4 conformations during the course of the REMD simulations. Only the oligomer backbones are shown for clarity.

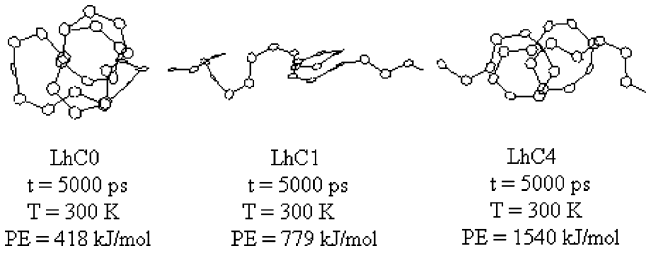

Figure 6. Postsimulation conformations for LhC0, LhC1, and LhC4 after 2 ns of canonical MD simulations. Only the oligomer backbones are shown for clarity.

three different oligomers (HhC0, HhC1, and HhC4) in Figure 7. We see that the R_g for the helix structures remains relatively constant over the course of the MD simulations. Similar results were found for the other two oligomers (HhC2 and HhC3), which are not shown. The R_g profiles for the LhC0 and LhC1 extended structures from canonical MD simulations show a rough terrain with peaks and valleys but remain relatively constant, indicating that these structures are trapped in local energy minima as shown in Figure 4. Similarly, the R_g profile for the LhC4 extended oligomer from the canonical MD simulation shows a steady decrease over the first 1.4 ns of trajectory until the structure becomes trapped in a local minimum energy state, yielding an average steady value for R_g. For the REMD simulations of the three extended structures, the R_g profiles show several spikes, while gradually reducing the average R_g. These spikes are indicative of neighboring replicas exchanging configurations between each other. Additionally, from Table 2, we see that the R_g values obtained from REMD simulations of LhC0, LhC1, and LhC4 are lower than those obtained from canonical MD simulations and closer to those obtained from the canonical MD simulation of the helical *m*-PPEs. This indicates that REMD enables the extended *m*-PPEs to attain lower energy conformations (i.e., more compact helical structures) than canonical MD methods.

The results of canonical MD simulations of five helical *m*-PPEs were analyzed to determine the effect of hydrophobicity and size of the side group, R, on the helix structure. The radius of gyration, R_g, was used to determine the degree of compactness of the final structures. Figure 8 shows the variation of R_g with side group, R. We observed that R_g passes through a minima where R = OC_2H_5, as the size of the R group is increased from R = H to OC_4H_9. Figure 8 also shows how the average helix inner diameter, D_H, varies with the size of R. In this study, D_H is defined as the distance between atoms C14 and C20 of the inner surface of each helix loop, and this distance was measured for each helix structure, using Weblab ViewerPro 3.20 software.[68]

Further, these measurements were corroborated by radial distribution functions between the C14 and C20 atoms. The radial distribution function for one of the helical structures, HhC3, is shown in Figure 9. Peak a, centered at 1.19 nm, corresponds to D_H. We observed that the variation in D_H with R group size followed the same trend as seen with the R_g data (Figure 8). This variation in relative compactness versus side group results from hydrophobic side chain−solvent repulsions (leading to more compact structures) and steric interactions within the helix core (leading to less compact structures).

The average helix pitch for the helical structures with and without the end loop residues being included in the calculations (i.e., P_H and P_{HC}, respectively) was also measured with Weblab ViewerPro 3.20 software.[68] The average helix pitch was determined by drawing a plane defined by three atoms for each helix turn and measuring the perpendicular distance between each plane. Several combinations of atoms (i.e., planes) were selected to determine the average distance between helical turns. Figure 10 shows a plot of P_H and P_{HC} versus side group, R. We observe that the helix pitch follows the same trend as R_g and D_H, with respect to the size of the R group. A closer examination of the data presented in Figure 10 reveals when R = H, OCH_3, or OC_2H_5, the average helix pitch when the end loop residues are included is higher than the values for when they are omitted. However, this trend is reversed once the R

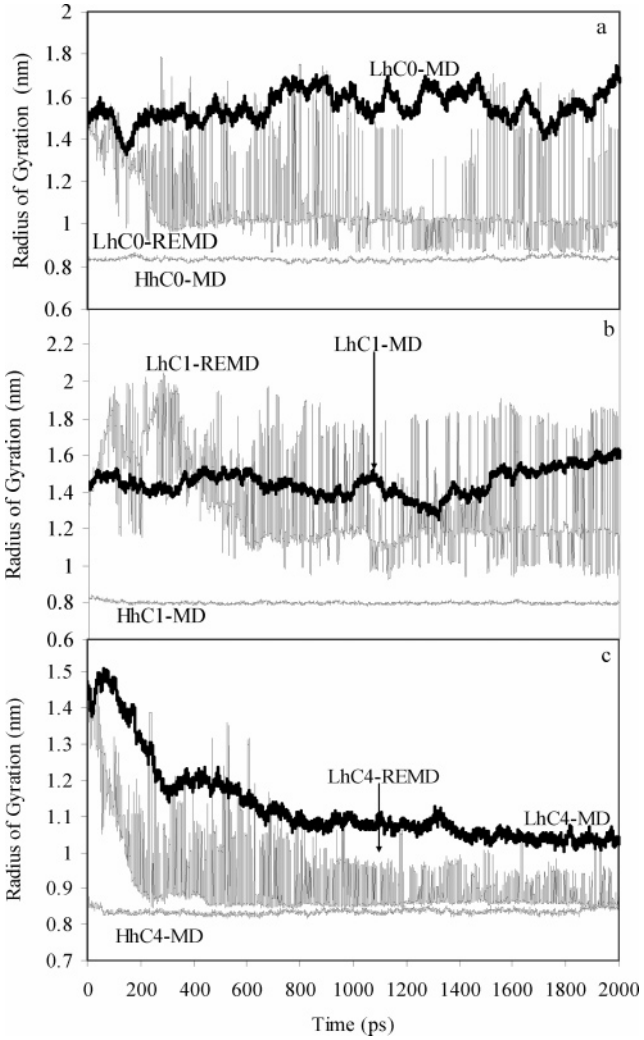

Figure 7. Time series of the radius of gyration, R_g, from REMD and MD for (a) extended (LhC0) and helical (HhC0) oligomers with R = H, (b) extended (LhC1) and helical (HhC1) oligomers with R = OCH_4, and (c) extended (LhC4) and helical (HhC4) oligomers with R = OC_4H_9. Only the first 2 ns of MD trajectory is shown.

TABLE 2: Radius of Gyration, R_g, from REMD and MD for (a) Extended (LhC0) and Helical (HhC0) Oligomers with R = H, (b) Extended (LhC1) and Helical (HhC1) Oligomers with R = OCH_4, and (c) Extended (LhC4) and Helical (HhC4) Oligomers with R = OC_4H_9, Averaged over the Last 10 ps of Trajectory

	radius of gyration, R_g (nm)	
structure	REMD[a]	MD[b]
LhC0	0.969 ± 0.057	1.068 ± 0.011
HhC0		0.826 ± 0.003
LhC1	0.973 ± 0.071	1.855 ± 0.025
HhC1		0.800 ± 0.004
LhC4	0.857 ± 0.008	1.250 ± 0.021
HhC4		0.832 ± 0.004

[a] Values after 2 ns of simulation time. [b] Values after 5 ns of simulation time.

group size is OC_3H_7 or greater, specifically, the difference between P_{HC} and P_H begins to widen. This can be explained by the fact that at lower R side group lengths (i.e., R = H through OC_2H_5), the repulsive forces between the solvent and the end loop residues of the helical oligomer are lower than the repulsive forces between R groups of adjacent turns of the helix, leading to higher values of P_H. For larger side groups (i.e., R = OC_3H_7 and OC_4H_9), the repulsive forces between the solvent and the end loop residues become large enough to compress the end loops of the helical structures inward, leading to a reduction in P_H.

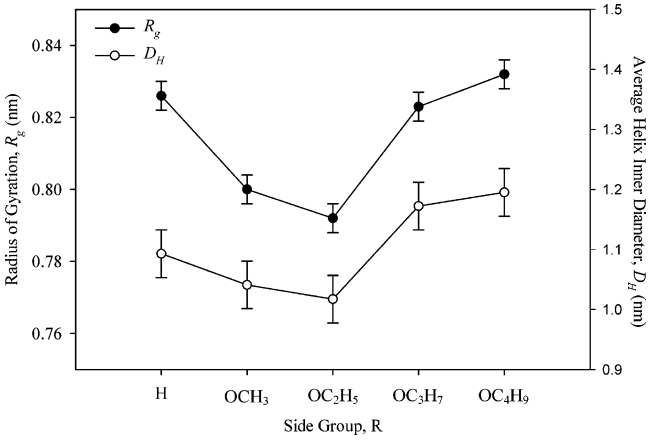

Figure 8. Radius of gyration, R_g, and average helix inner diameter, D_H, versus side group, R, obtained from MD simulations of the helical *m*-PPEs.

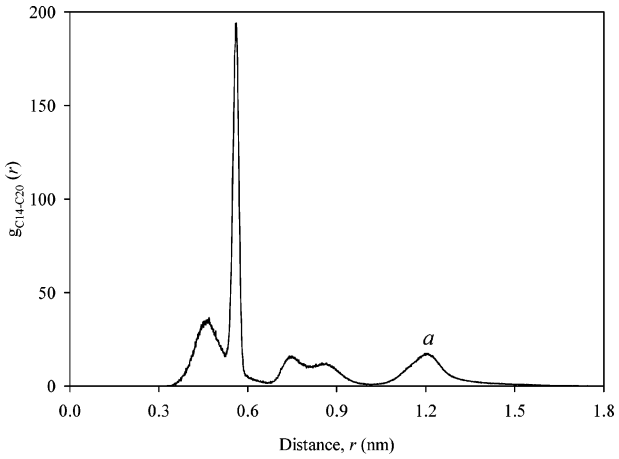

Figure 9. Computed radial distribution function, $g(r)$, between the C14 and C20 atoms of the helical *m*-PPE oligomer, HhC3.

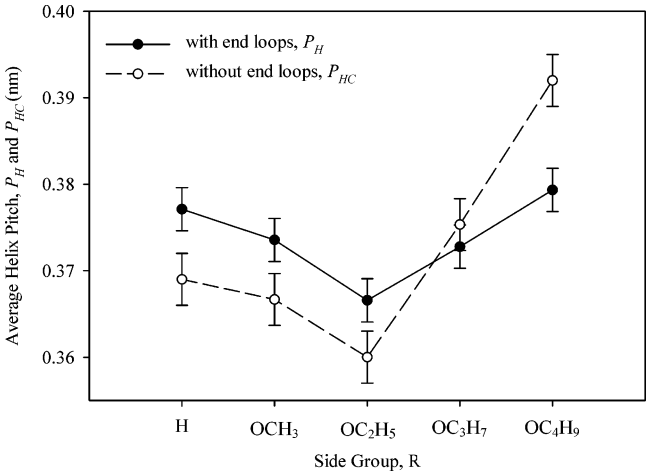

Figure 10. Average helix pitch, P_H and P_{HC}, versus side group, R, obtained from MD simulations of the helical *m*-PPEs.

The initial increase in relative compactness of the helical structure (i.e., lower R_g, D_H, P_H, and P_{HC} values) when the side group R length is increased from R = H through OC_2H_5 is due to the fact that the repulsive forces between the hydrophobic alkoxy side groups of the HhC1 and HhC2 oligomers and the polar solvent (water) are greater than the steric interactions

TABLE 3: Potential Energy for the Helix, Extended, and Coiled Conformations of the *m*-PPE Oligomer with R = H, OCH_3, OC_2H_5, OC_3H_7, and OC_4H_9, after 5 ns of MD Simulations, Averaged over the Last 10 ps of Trajectory

	potential energy (kJ/mol)		
side group R	extended[a]	coiled[b]	helix[c]
H	924.53	418 ± 32	201 ± 32
OCH_3	1451.08	779 ± 42	466 ± 38
OC_2H_5	1774.15	1335 ± 38	1023 ± 35
OC_3H_7	2153.17	1566 ± 70	1353 ± 35
OC_4H_9	2502.40	1540 ± 45	1339 ± 46

[a] Presimulation. [b] Postsimulation extended structure. [c] Postsimulation.

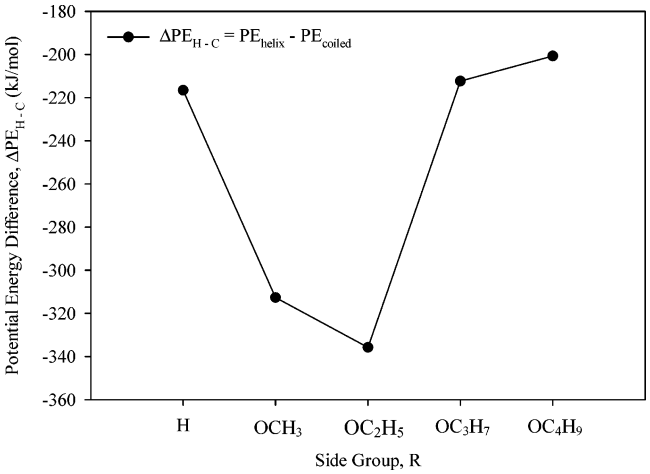

Figure 11. Potential energy difference, ΔPE_{H-C}, versus side group, R, obtained from MD simulations of the extended and helical *m*-PPEs.

between the alkoxy groups within the helix core. As the size of the alkoxy side group is increased further from 2 carbon atoms to 4 carbon atoms long, the steric interactions begin to have a more dominant effect, resulting in less compact structures (i.e., higher R_g, D_H, P_H, and P_{HC} values). Hence, it is important to state that as the size of the R side group is increased to more than 4 carbon atoms long, it is less likely that the helical structure will be the minimum energy conformation. This is due to the fact that it becomes increasingly difficult for the *m*-PPE oligomer to fold into a helical conformation in aqueous solvent because the alkoxy side chains will become too large for the interior cavity of the helix.

To gain additional insight into the effects of side chain structures on the driving force for folding, we calculated the potential energy difference for the helix-coil transition. This potential energy difference, ΔPE_{H-C}, is defined as the potential energy of the oligomer in the helix (postsimulation) conformation minus the potential energy of the randomly coiled (postsimulation extended) structure (i.e, $PE_{helix} - PE_{coiled}$). Table 3 shows the potential energy for the helix, extended, and coiled conformations of the *m*-PPE oligomer after 5 ns of MD simulations, while Figure 11 illustrates the variation of ΔPE_{H-C} versus polymer side group R. We see that the plot is similar to Figures 8 and 10. ΔPE_{H-C} passes through a minimum in energy when R = OC_2H_5 as the length of the side group R is increased from H to an alkoxy group that is 4 carbon atoms long. As mentioned previously, this can be explained by the fact that when R = OC_2H_5, repulsive forces between the oligomer side group and solvent are significant yet the steric interaction of the R side groups is not a major factor. As the size of R is increased above R = OC_2H_5, unfavorable steric interactions cause the energy of the helix conformation to be increased, which consequently reduces the energy difference between helix and coiled conformations.

Conclusions

In this study, we investigated the folding behavior of amine-functionalized *m*-PPE oligomers in an extended conformation in water, using replica exchange and canonical MD simulation techniques. We studied five different extended *m*-PPE oligomers that varied only in size and hydrophobicity of side groups. Our results showed that the REMD method is a more useful technique than canonical MD in predicting the helical conformation of *m*-PPEs in water, from an extended *m*-PPE structure, in the same simulation time. Additionally, we observed from canonical MD simulations of the helical *m*-PPEs that the relative compactness of the helix structure reaches a minima and then increases as the length of the hydrophobic side group is increased. Our data suggest that the crossover point where helical structures become less compact as the side chain length increases occurs with functional groups longer than OC_2H_5.

Acknowledgment. The authors acknowledge the financial support of the National Science Foundation (NSF) (CAREER 9985022) and the ERC Program of NSF under Award No. EEC-9731680. The authors also acknowledge the assistance of Walter L. Ash of the Department of Biological Sciences, University of Calgary, for providing the GROMACS-REMD Code, and Jay McAliley of the Department of Chemical Engineering, Clemson University, and the Clemson University Beowulf Supercomputing Administrator, Tim Shelling, for their assistance in modifying the code to our specifications.

References and Notes

(1) Anfinsen, C. B. *Science* **1973**, *181*, 223−230.
(2) Nelson, J. C.; Moore, J. S.; Wolynes, P. G.; Saven, J. G. *Science* **1997**, *277*, 1793−1796.
(3) Dill, K. A. *Biochemistry* **1990**, *29*, 7133−7155.
(4) Fersht, A. R. *Structure and Mechanism in Protein Science*; W. H. Freeman and Company: New York, 1999.
(5) Blanco, F. J.; Serrano, L. *Eur. J. Biochem.* **1995**, *230*, 634−649.
(6) Zhou, R.; Berne, B. J.; Germain, R. *Proc. Natl. Acad. Sci. U.S.A.* **2001**, *98*, 14931−14936.
(7) Zhou, Y.; Karplus, M. *Nature* **1999**, *40*, 400−403.
(8) Brooks, C. L.; Gruebele, M.; Onuchic, J. N.; Wolynes, P. G. *Proc. Natl. Acad. Sci. U.S.A.* **1998**, *95*, 11037−11038.
(9) Munoz, V.; Henry, E. R.; Hofrichter, J.; Eaton, W. A. *Proc. Natl. Acad. Sci. U.S.A.* **1998**, *95*, 5872−5879.
(10) Zhou, R. *Proteins*: *Struct. Funct. Genet.* **2003**, *53*, 148−161.
(11) Suenaga, A. *J. Mol. Struct.* (*THEOCHEM*) **2003**, *634*, 235−241.
(12) Prusiner, S. B. *Science* **1997**, *278*, 245−251.
(13) Yankner, B. A.; Dawes, L. R.; Fisher, S.; Villa-Komaroff, L.; Oster-Granite, M. L.; Neve, R. L. *Science* **1989**, *245*, 417−420.
(14) Prince, R. B.; Saven, J. G.; Wolynes, P. G.; Moore, J. S. *J. Am. Chem. Soc.* **1999**, *121*, 3114−3121.
(15) Stone, M. T.; Moore, J. S. *Org. Lett.* **2004**, *6*, 469−472.
(16) Goto, H.; Heemstra, J. M.; Hill, D. J.; Moore, J. S. *Org. Lett.* **2004**, *6*, 889−892.
(17) Goto, K.; Moore, J. S. *Org. Lett.* **2005**, *7*, 1683−1686.
(18) Arnt, L.; Tew, G. N. *J. Am. Chem. Soc.* **2002**, *124*, 7664−7665.
(19) Arnt, L.; Tew, G. N. *Macromolecules* **2004**, *37*, 1283−1288.
(20) Breitenkamp, R. B.; Arnt, L.; Tew, G. N. *Polym. Adv. Technol.* **2005**, *16*, 189−194.
(21) Tan, C. Y.; Pinto, M. R.; Kose M. E.; Ghiviriga, I.; Schanze, K. S. *Adv. Mater.* **2004**, *16*, 1208−1212.
(22) Inouye, M.; Waki, M.; Abe, H. *J. Am. Chem. Soc.* **2004**, *126*, 2022−2027.
(23) Orita, A.; Nakano, T.; An, D. L.; Tanikawa, K.; Wakamatsu, K.; Otera, J. *J. Am. Chem. Soc.* **2004**, *126*, 10389−10396.
(24) Blatchly, R. A.; Tew, G. N. *J. Org. Chem.* **2003**, *68*, 8780−8785.
(25) Jones, T. V.; Blatchly, R. A.; Tew, G. N. *Org. Lett.* **2003**, *5*, 3297−3299.
(26) Shotwell, S.; Windschief, P. M.; Smith, M. D.; Bunz, U. H. F. *Org. Lett.* **2004**, *6*, 4151−4154.
(27) Grubbs, R. H.; Kratz, D. *Chem. Ber. Recl.* **1993**, *126*, 149−157.

(28) Leach, A. R. *Molecular Modelling*: *Principles and Applications*, 2nd ed.; Prentice Hall: Essex, UK, 2001.
(29) Jensen, F. *Introduction to Computational Chemistry*; John Wiley and Sons: London, UK, 1999.
(30) Mitsutake, A.; Sugita, Y.; Okamoto, Y. *Biopolymers* **2001**, *60*, 96−123.
(31) Hansmann, U. H. E. *Chem. Phys. Lett.* **1997**, *281*, 140−150.
(32) Hansmann, U. H. E.; Okamoto, Y. *J. Comput. Chem.* **1993**, *14*, 1333−1338.
(33) Berg, B. A.; Neuhaus, T. *Phys. Lett. B* **1991**, *267*, 249−253.
(34) Berg, B. A.; Neuhaus, T. *Phys. Rev. Lett.* **1992**, *68*, 9−12.
(35) Nakajima, N.; Nakamura, H.; Kidera, A. *J. Phys. Chem. B* **1997**, *101*, 817−824.
(36) Kirkpatrick, S.; Gelatt, C. D., Jr.; Vecchi, M. P. *Science* **1983**, *220*, 671−680.
(37) Naidoo, K. J.; Brady, J. W. *Chem. Phys.* **1997**, *224*, 263−273.
(38) Wilson, S. R.; Cui, W.; Moskowitz, J. W.; Schmidt, K. E. *J. Comput. Chem.* **1991**, *12*, 342−349.
(39) Sugita, Y.; Okamoto, Y. *Chem. Phys. Lett.* **1999**, *314*, 141−151.
(40) Metropolis, N.; Rosenluth, A. W.; Rosenbluth, M. N.; Teller, A. H.; Teller, E. *J. Chem. Phys.* **1953**, *21*, 1087−1092.
(41) Rhee, Y. M.; Pande, V. S. *Biophys. J.* **2003**, *84*, 775−786.
(42) Rao, F.; Caflisch, A. *J. Chem. Phys.* **2003**, *119*, 4035−4042.
(43) Elmer, S.; Pande, S. V. *J. Phys. Chem. B.* **2001**, *105*, 482−485.
(44) Sen, S. *J. Phys. Chem. B.* **2002** *106*, 11343−11350.
(45) Lee, O.; Saven, G. S. *J. Phys. Chem. B* **2004**, *108*, 11988−11994.
(46) Adisa, B.; Bruce, D. A. *J. Phys. Chem. B* **2005**, *109*, 7548−7556.
(47) Berendsen, H. J. C.; van der Spoel, D.; van Drunen, R. *Comput. Phys. Commun.* **1995**, *91*, 43−56.
(48) Berendsen, H. J. C.; van der Spoel, D.; van Drunen, R.; van Buuren, A. R.; Apol, E.; Meulenhoff, P. J.; Tieleman, D. P.; Sijbers, A. L. T. M.; Feenstra, K. A.; Lindahl, E.; Hess, B. *Gromacs User Manual*, version 3.1.1; University of Groningen: Groningen, The Netherlands, 2002.
(49) Lindahl, E.; Hess, B.; van der Spoel, D. *J. Mol. Model.* **2001**, *7*, 306−317.
(50) Jorgensen, W. L.; Maxwell, D. S.; Tirado-Rives, J. *J. Am. Chem. Soc.* **1996**, *118*, 11225−11236.
(51) Rizzo, R. C.; Jorgensen, W. L. *J. Am. Chem. Soc.* **1999**, *121*, 4827−4836.
(52) Price, M. L. P.; Ostrovsky, D.; Jorgensen, W. L. *J. Comput. Chem.* **2001**, *22*, 1340−1352.
(53) Jorgensen, W. L.; Tirado-Rives, J. *J. Am. Chem. Soc.* **1988**, *110*, 1657−1666.
(54) *Materials Studio*, version 2.1; Accelrys Inc., 2001.
(55) Eisenberg, D.; McLachlan, A. D. *Nature* **1986**, *319*, 199−203.
(56) Berendsen, H. J. C.; Postma, J. P. M.; von Gunsteren, W. F.; Hermans, J. In *Intermolecular Forces*; Pullman, B., Ed.; Reidel: Dordrecht, The Netherlands, 1981.
(57) Nocedal, J. *Math. Comput.* **1980**, *35*, 773−782.
(58) *Jaguar 4.0*; Schrodinger, Inc.: Portland, OR, 2000.
(59) Becke, A. D. *J. Chem. Phys.* **1993**, *98*, 5648−5652.
(60) Lee, C.; Yang, W.; Parr, R. G. *Phys. Rev.* B **1988**, *37*, 785−789.
(61) Pople, J. A.; Krishnan, R.; Binkley, J. S.; Seeger, R. *J. Chem. Phys.* **1980**, *72*, 650−654.
(62) Okuyama, K.; Hasegawa, T.; Ito, M.; Mikami, N. *J. Phys. Chem.* **1984**, *88*, 1711−1716.
(63) Hockney, R. W. *Methods Phys.* **1970**, *9*, 136−211.
(64) Potter, D. *Computational Physics*; Wiley and Sons: London, UK, 1973.
(65) Berendsen, H. J. C.; Postma, J. P. M.; DiNola, A.; Haak, J. R. *J. Chem. Phys.* **1984**, *81*, 3684−3690.
(66) Hess, B.; Bekker, H.; Berendsen, H. J. C.; Fraaije, J. G. E. M. *J. Comput. Chem.* **1997**, *18*, 1463−1472.
(67) Miyamoto, S.; Kollman, P. A. *J. Comput. Chem.* **1992**, *13*, 952−962.
(68) *Weblab ViewerPro*, version 3.20; Molecular Simulations Inc.: San Diego, CA, 1998.